Available online at www.sciencedirect.com
SCIENCE DIRECT
Polymer 47 (2006) 3351–3362
polymer
www.elsevier.com/locate/polymer

Structures and phase transformations of odd-numbered asymmetric main-chain liquid crystalline polyesters

Kwang-Un Jeong, Brian S. Knapp, Jason J. Ge, Matthew J. Graham, Yingfeng Tu, Siwei Leng, Huiming Xiong, Frank W. Harris, Stephen Z.D. Cheng *

Department of Polymer Science, Maurice Morton Institute, The University of Akron, Akron, OH 44325-3909, USA

Received 3 November 2005; received in revised form 4 March 2006; accepted 6 March 2006
Available online 3 April 2006

Abstract

Two new asymmetric odd-numbered main-chain liquid crystalline (LC) polyesters (BPE-C*n*) were synthesized through the condensation polymerization of A–B type asymmetric α,ω-carboxylic acid–hydroxyl terminated monomers with odd-numbers of methylene units in the spacers (BPCA-C*n*-P*m*OH, where $n=7$ and 9). The phase behaviors and structures of these odd-numbered BPE-C*n* samples were characterized using the combined techniques of differential scanning calorimetry (DSC), wide angle X-ray diffraction (WAXD), selected area electron diffraction (SAED) and polarized light microscopy (PLM). One-dimensional (1D) powder WAXD results at different temperatures combined with DSC results revealed that during cooling these two polyesters enter a low-ordered LC phase before developing a crystalline phase at lower temperatures. Based on 2D WAXD of oriented fiber patterns, the low ordered LC phase of odd-numbered BPE-C*n* was identified to be a smectic A (SmA) phase, which was constructed by each chemical repeating unit along the fiber drawn direction. The crystalline structures were determined to be monoclinic unit cells (K_M). However, BPE-C7 possessed a $\gamma=87°$, while BPE-C9 had a $\beta=100°$. These crystalline structure identifications were also confirmed by SAED from single crystals. Two-chain packing models of the K_M phases with four chemical repeating units were proposed on the basis of the experimental diffraction patterns. The different structures were attributed to the interplay between the mesogenic group ordering propensity and the chain constraints dictated by the methylene spacer and the meta-linkage at the end of mesogen. In the ordered phases of these two odd-numbered BPE-C*n* polyesters, aromatic mesogenic groups are more or less parallel to each other along the chain with small angles of deviation from the *c*-axis of the crystal lattice, different from those large zigzag conformation structures in even-numbered BPE-C*n* crystals. Crystallographic calculations of these two unit cell structures indicated that the neighboring chains in the crystals are translated along the *c*-axis (in the case of BPE-C9) or twisted away from the *b*-axis (in the case of BPE-C7) in order to incorporate both of the bend attributed to the odd-numbered methylene spacers and of the configurational meta-linkage at the end of mesogens. The simulated diffractions based on these calculations qualitatively agreed with the experimental observations. The phase identifications were also supported by the observed texture changes in PLM.

Keywords: Liquid crystalline polymers; Morphology; Phase structures

1. Introduction

Due to the anisotropic properties and the self-assembling capabilities of liquid crystalline (LC) materials, main-chain LC polymers have been used in a range of mechanical, electrical, optical and biological applications. In order to tune these properties, main-chain LC polymers, comprised of flexible alkylene spacers between rigid and controlled aromatic units, with various chemical structures and molecular architectures for both mesogenic groups and flexible spacers have been designed [1–11]. It is common to tailor LC stabilities by selecting different mesogenic groups, varying the location of the mesogens, and altering the lengths and types of flexible spacers in the LC polymers. Forming their liquid crystalline phases is dependent of the configuration of the meta- and para-linkages in the mesogenic groups. The spacer length can cause periodic changes in the thermodynamic properties of a material (in particular, the transition properties) based on whether there are an even or odd number of unit in the LC polymer spacers. These changes have been termed the odd–even effect.

Recently, the odd–even effect has reported to extend to other structural and morphological phenomena. For example, a series

* Corresponding author.
E-mail address: scheng@uakron.edu (S.Z.D. Cheng).

0032-3861/$ - see front matter © 2006 Elsevier Ltd. All rights reserved.
doi:10.1016/j.polymer.2006.03.025

of BB-*n* polyesters (*n*: the number of methylene units), synthesized via the melt condensation polymerization of *p*,*p*-bibenzoic acid (A–A type) and alkylene glycols (B–B type) monomers, demonstrated the structural odd–even effect. The even-numbered BB-*n* polyesters exhibited a low-ordered smectic A (SmA) phase, but the mesophase of the odd-numbered ones was identified to be an anticlinically tilted smectic C (SmC_A) phase layer-by-layer [12–18]. As an example of the morphological odd–even effect, a series of chiral polyesters were synthesized via the solution condensation polymerization of non-racemic chiral A–B type monomers, (*R*)-(−)-4′-{ω-[2-(*p*-hydroxy-*o*-nitrophenyloxy)-1-propyloxy]-1-nonyloxy}-4-biphenyl carboxylic acid [PET-(*R**)-*n*, *n*: the number of methylene units]. This series of polyesters can form double-twisted helical single crystals, and the handednesses of the single crystals are determined by the number of methylene units in the spacers. This is a morphological odd–even effect: the PET(*R**)-*n* polyesters containing the identical *R** chiral center but having *n* = odd developed right-handed helical crystals while *n* = even grew left-handed helical crystals [19–27].

We recently reported that a three-dimensional (3D) helical supramolecular structure formed in a synclinically tilted smectic C (SmC_S) phase of the achiral α,ω-carboxylic acid–hydroxyl terminated series of compounds with different methylene spacer units (BPCA-C*n*-P*m*OH, *n* = 6–10) [28,29]. When this series of A–B type asymmetric BPCA-C*n*-P*m*OH compounds was polymerized, the corresponding polyesters (BPE-C*n*) having a bend due to the meta-linkage in its chemical structure were obtained. In the case of the even-numbered BPE-C*n* polyester, three phases were identified as the low-ordered SmC_A phase, the highly ordered SmH_A crystal phase, and the crystalline orthorhombic K_O phase [30]. Of particular interest is that in all of these ordered phases, the even-numbered BPE-C*n* chains retain the large zigzag conformation, which becomes the basic building block of these ordered structures.

To extend the investigation of the odd–even effect from the monomer to the polymer, we synthesized two asymmetric odd-numbered main-chain LC polyesters (BPE-C*n*, *n* = 7 and 9) containing both a configurational bend because of the meta-linkage and a conformational bend because of the odd-numbered methylene units, and studied their phase behaviors and structures to understand the effects of both the bends. Differential scanning calorimetry (DSC) experiments were first utilized to detect the thermal transitions in these two BPE-C*n* polyesters. The phase structures of these two BPE-C*n* were identified by structurally sensitive experiments, such as wide angle X-ray diffraction (WAXD) and selected area electron diffraction (SAED). Their molecular conformations and packing schemes were deduced from structural characterization and supported by computer simulations. The phase morphologies in LC and in crystalline phases were then investigated via polarized light microscopy (PLM). From this research, we achieved an understanding of the mechanisms involved in the structural and morphological odd–even effect.

2. Experimental section

2.1. Materials and sample preparations

Two asymmetric main-chain LC polyesters (BPE-C*n*) with an odd-number of methylene units (*n* = 7 and 9) were synthesized via the condensation polymerization of the A–B type asymmetric BPCA-C*n*-P*m*OH (where *n* is 7 and 9), which were prepared via four step substitution reactions as reported before [30,31]. The general chemical structure of these odd-numbered BPE-C*n* polyesters is

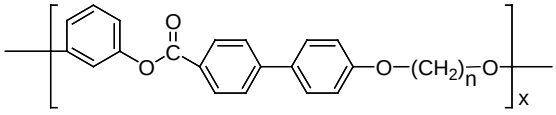

BPE-Cn, n = 7 and 9

Chemical structures of the BPCA-C*n*-P*m*OHs and their corresponding polyesters (BPE-C*n*) were confirmed by Fourier transform infrared spectroscopy and solution proton and carbon-13 nuclear magnetic resonance. The number-average molecular weights of BPE-C*n* (*n* = odd numbers) were determined by gel permeation chromatography based on polystyrene standards and intrinsic viscosity measurement, and they ranged between 25,000 and 35,000 g/mol with polydispersities between 2.0 and 2.5. The thermal gravimetric analysis showed that BPE-C*n* polyesters were thermally stable. The polymer underwent 2 and 5% weight loss at 360 and 390 °C, respectively, at a heating rate of 10 ° C/min under a dry nitrogen atmosphere. A more detailed description of the synthetic and purification processes for the monomers and their corresponding polyesters can be found in a Ref. [31].

The samples were kept in vacuum before carrying out characterization and analysis. For differential scanning calorimetry (DSC) experiments, the sample weight was about 2.0 mg and the pan weights were kept constant at a precision of ±0.001 mg. To observe the evolution of different phase structures, film samples with a thickness of 1 mm were prepared by melting the polymer powders for one-dimensional (1D) WAXD powder experiments. Oriented fibers drawn from the LC phase were annealed at different temperatures in order to determine phase structures using 2D WAXD experiments. The samples used in PLM observations were melt-pressed between two glass slides with a typical gap thickness of 10 μm. Thin film samples were prepared for TEM via solution casting from a 0.05% (w/v) chloroform solution onto carbon-coated mica with thicknesses of 50–150 nm. After crystallization, the films were floated onto the water surface and recovered using the TEM copper grids.

2.2. Equipment and experiments

The thermal behaviors of the phase transitions were studied using a Perkin–Elmer PYRIS Diamond DSC with an Intracooler 2P apparatus. The temperatures and heat flows were calibrated using material standards at cooling and heating rates ranging from 2.5 to 40 °C/min. The heating experiments

always preceded the cooling experiments in order to eliminate previous thermal histories, and the cooling and heating rates were always kept identical. The transition temperatures were determined by measuring the onset and peak temperatures from both the cooling and heating scans at different rates. During cooling, the onset temperature was determined on the high-temperature side, and upon heating the onset temperature was determined on the low-temperature side of the transition peaks.

Phase structures and transformations were identified using 1D WAXD powder experiments. These were conducted in the transmission mode of a Rigaku 12 kW rotating-anode X-ray (Cu K_α radiation) generator coupled to a diffractometer. The diffraction peak positions and widths were calibrated with silicon crystals of known crystal size in the high 2θ-angle region ($>15°$) and silver behenate in the low 2θ-angle region. A hot stage was coupled to the diffractometer in order to study the LC structural evolutions during cooling and heating. The temperature of this hot stage was calibrated to be within ± 1 °C. Samples were scanned between 1.5 and 35° at a scanning rate of 4°/min. The oriented fiber 2D WAXD patterns were obtained using a Rigaku X-ray imaging system with an 18 kW rotating anode X-ray generator. A hot stage was also used to obtain diffraction patterns from the crystal and LC structures at different temperatures. The patterns were recorded on an image plate (Rigaku, R-AXIS-IV). A 30 min exposure time was required for a high-quality pattern. In both 1 and 2D WAXD experiments, background scattering was subtracted from the sample scans.

TEM (FEI Tacnai 12) experiments were carried out to examine crystal morphology on the nanometer scale using an accelerating voltage of 120 kV. SAED patterns of the sample from different zones were obtained using a tilting stage to determine the crystal unit-cell symmetry and dimensions. The camera length was set at 2.1 m and calibration of the SAED spacing smaller than 0.384 nm was carried out using evaporated thallous chloride, which has a largest first-order spacing diffraction of 0.384 nm. Spacing values larger than 0.384 nm were calibrated by doubling the d-spacing values of the first-order diffractions. Morphological observation of the phases on the micrometer scale at different temperatures were conducted on an Olympus (BH-2) PLM coupled with a Mettler heating stage (FP-90).

Density measurements were carried out at room temperature using a Guy-Lussac type specific gravity bottle (10 mL), which was calibrated using ASTM D 369 method. Mixed solutions of carbon tetrachloride/hexane were used to find the density of crystallized fiber samples. The measured density value was used to judge the number of chemical repeating units in a crystalline unit cell.

Crystallographic simulation was performed using Cerius^2 (Version 4.6) simulation software from Accelrys utilizing the COMPASS force field. The lowest energy conformation of the single polymer chain was chosen as the starting conformation. Basic unit cell parameters determined by crystallographic experimental data from 2D WAXD and SAED experiments were used in order to build the crystal unit cell. The positions of atoms in this unit cell were judged by comparing their calculated diffraction patterns with those of experiments.

3. Results and discussion

3.1. Thermodynamic transitions and their corresponding structural evolutions

Fig. 1(a) and (b) shows sets of DSC cooling and subsequent heating thermal diagrams for asymmetric main-chain BPE-Cn ($n=6$–10) at a rate of 2.5 °C/min. Two thermal transition processes are clearly observed in the odd-numbered BPE-Cn samples while three transition processes for the even-numbered are observed. The BPE-Cn samples containing the longer methylene spacers exhibit lower transition temperatures, but the odd–even effect in their isotropic transition temperature (T_i) is not obvious. This could be due to the differences of ordered structures between odd- and even-numbered BPE-Cn below the T_i, which will be discussed in detail in the structure identification section of this publication. Particularly, structures and phase transformations of the odd-numbered BPE-Cn ($n=7$ and 9) will be discussed, and compared with those of even-numbered BPE-Cn polyesters [30]. During cooling, the two transition processes are observed at 195 and 187 °C in the case of BPE-C7, and at 181 and

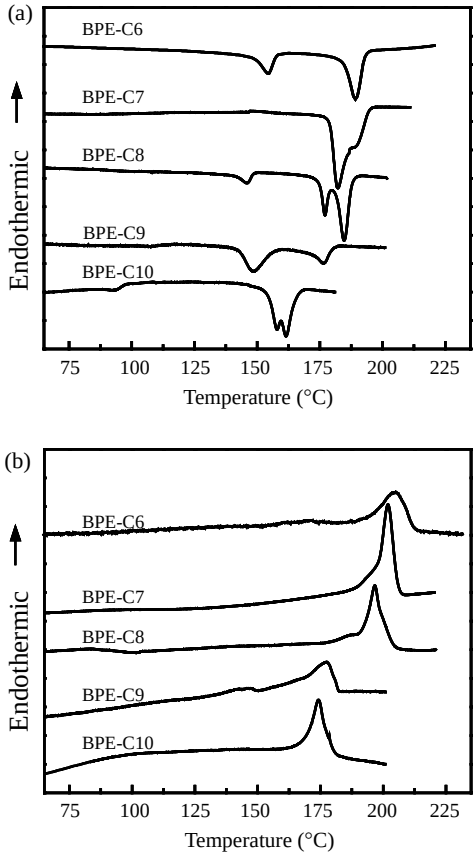

Fig. 1. Two sets of DSC cooling (a) and subsequent heating (b) thermal diagrams for BPE-Cn ($n=6$–10) samples at a rate of 2.5 °C/min.

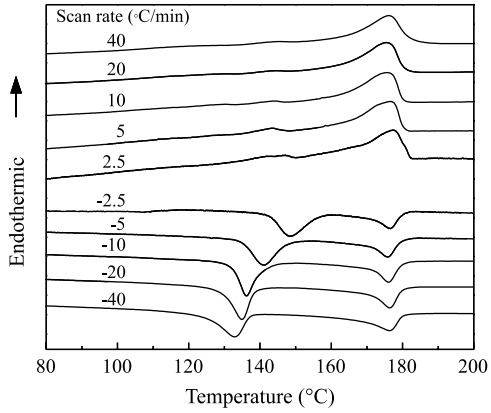

Fig. 2. Set of DSC cooling and subsequent heating thermal diagrams of BPE-C9 at cooling and heating rates ranging from 2.5 to 40 °C/min.

160 °C for BPE-C9. These two transition processes are also detected during heating at the same rate, yet the transitions overlap.

Fig. 2 shows two sets of DSC cooling and subsequent heating diagrams for BPE-C9 at different rates ranging from 2.5 to 40 °C/min, as an example for these two odd-numbered BPE-C*n* polyesters. The heats of transition for the two thermal transitions measured during cooling at 2.5 °C/min are 3.2 kJ/mol at 181 °C and 6.5 kJ/mol at 160 °C, respectively. For the high-temperature transition, the heat of transition and the onset transition temperature at the high-temperature side do not exhibit cooling rate dependence. This indicates that the high-temperature transition takes place close to thermodynamic equilibrium, and it may be associated with the transitions between an isotropic melt (I) and a low ordered LC phase [28–35]. In contrast, the heat of transition (6.5 kJ/mol) at the lower transition temperature and its onset transition temperature are cooling rate dependent, which is often observed during polymer crystallization processes.

Although DSC experiments are sensitive to heat absorption and release events, this technique cannot provide direct information about structural changes. Therefore, 1D WAXD experiments at different temperatures were combined with DSC results to identify the corresponding structural evolutions. Fig. 3(a) shows a set of 1D WAXD powder patterns at different temperatures while cooling at a rate of 2.5 °C/min for BPE-C9. In this figure, structures on two different length scales can be identified. One is on the nanometer scale in the low 2θ-angle region between 1.5 and 9°, and another on the sub-nanometer scale can be identified between 9 and 35°. The 1D WAXD powder patterns in Fig. 3(a) show two-phase transitions, and they agree well with the observations in the DSC cooling diagrams (Fig. 2). At temperatures above 181 °C, BPE-C9 is in the I phase exhibiting only an amorphous halo at $2\theta = 18.6°$ ($d = 0.477$ nm). When the temperature reached 181 °C, a low 2θ-angle diffraction at $2\theta = 3.70°$ ($d = 2.39$ nm) starts to develop. This usually indicates the formation of the layer structure of a smectic LC phase. In addition to the layer diffraction in the low 2θ-angle region, the amorphous halo

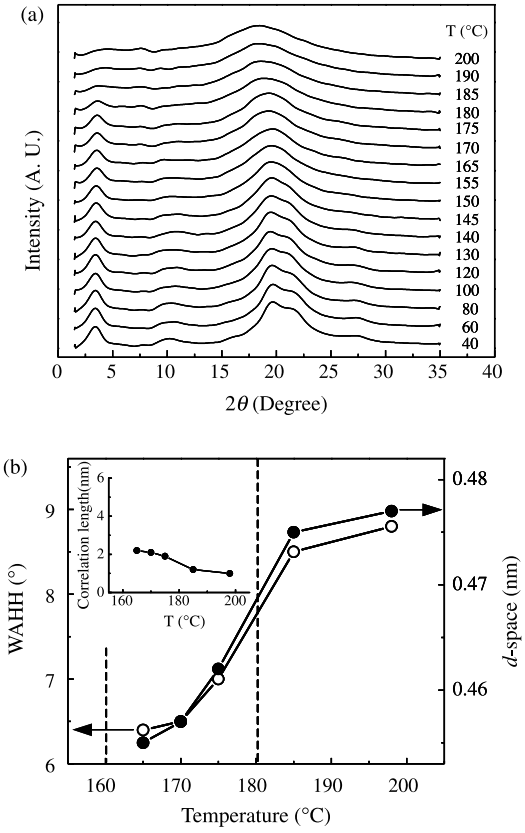

Fig. 3. Set of 1D WAXD powder patterns of BPE-C9 during cooling at a rate of 2.5 °C/min at different temperatures (a). The relationship of the *d*-spacing of the high 2θ-angle scattering halo and the correlation length of the scattering halo of BPE-C9 at different temperatures above 160 °C (b). The correlation lengths were calculated based on the Scherrer equation and shown as an inset of Fig. 3(b). The vertical dash-lines are indications of the thermal transitions based on the DSC cooling rate.

at $2\theta = 18.6°$ (*d*-spacing = 0.477 nm) suddenly shifts to $2\theta = 19.4°$ (*d*-spacing = 0.458 nm) in the high 2θ-angle region. Below 160 °C, which corresponds to the lower temperature thermal transition in Fig. 2, relatively sharp reflections develop in the high 2θ-angle region, and the diffraction peaks in the low 2θ-angle region are also enhanced as shown in Fig. 3(a).

The structural changes of BPE-C9 in Fig. 3(a) can also be characterized by the *d*-spacing changes and the changes in the width at half-height (WAHH) of the high 2θ-angle scattering halo with respect to temperatures above 160 °C. The correlation lengths of this halo can be calculated using the WAHH data based on the Scherrer equation. The results are shown in Fig. 3(b). For example, a correlation length is estimated to be between 1.8 and 2.2 nm below 181 °C (see the inset of Fig. 3(b)), indicating a liquid-like, short-range order in the lateral molecular packing in the smectic layers [32–37]. The vertical dash-lines are indications of the thermal transitions based on the DSC cooling results. The changes in these structural parameters correspond well to the thermal transitions observed in DSC. The 1D WAXD powder patterns during heating also agree well with the thermal transitions observed in the DSC heating results.

3.2. Identifications of crystal structures

In order to obtain detailed structural determination and symmetry, 2D WAXD experiments on oriented BPE-C*n* samples were conducted. A 2D WAXD pattern for BPE-C9, from a fiber drawn in the LC phase at 177 °C and annealed at 158 °C for 1 day, is shown in Fig. 4(a). This pattern exhibits diffractions on the equator and in the quadrants, but not on the meridian. As indicated in this figure, the a^*- and b^*-axes are assigned to the equator, and the c^*-axis is $\pm 10°$ away from the meridian (fiber drawn direction). The $\pm 10°$ angle was evaluated by an azimuthal scan along a radial angle range between 3.0 and 5.0°. On the equator of this fiber pattern, three diffractions located at $2\theta = 19.1°$ ($d = 0.47$ nm), 22.1° ($d = 0.40$ nm) and 27.1° ($d = 0.33$ nm) can be identified. Based on the triangulation method of building a 2D a^*b^*-lattice of the unit cell [38], they can be assigned as the (110), (020) and (120) planes, respectively, and the γ angle is calculated to be 90°. In the low 2θ-angle region of this fiber pattern, two pairs of strong diffraction spots appear at $2\theta = 3.56°$ ($d = 2.48$ nm) in the quadrants with higher order diffractions at $2\theta = 7.13°$ ($d = 1.24$ nm). Both of them are located at $\pm 10°$ away from the meridian direction. They can be assigned as the (002) and (004) diffractions, therefore, the β angle should be 100°. Careful structural analysis gives a monoclinic unit cell with dimensions of $a = 0.58$ nm, $b = 0.80$ nm, $c = 5.04$ nm, $\alpha = \gamma = 90°$, and $\beta = 100°$ via the refinement of the reciprocal lattice using a procedure developed in our laboratory [38], and this phase is abbreviated to be the K_M phase. Table 1 lists the experimentally observed and the calculated 2θ values and the d-spacings based on this unit cell lattice. With two chains (four chemical repeating units) in this monoclinic unit cell, its calculated crystallographic density is 1.24 g/cm^3. The experimentally observed density is 1.22 g/cm^3, which fits well with the calculated data. A schematic two-chain unit cell model for this K_M crystalline phase of BPE-C9 is shown in Fig. 4(b). Compared with the crystalline chain-packing model of the even-numbered BPE-C*n* in which each chain keeps the large zigzag conformation [30], aromatic mesogenic groups in BPE-C9 are more or less parallel to each other, as illustrated in Fig. 4(b). Note that in general, the odd-numbered BB-*n* polyesters show a zigzag chain conformation along the polymer chain, while the mesogens are parallel in case of the even-numbered if the

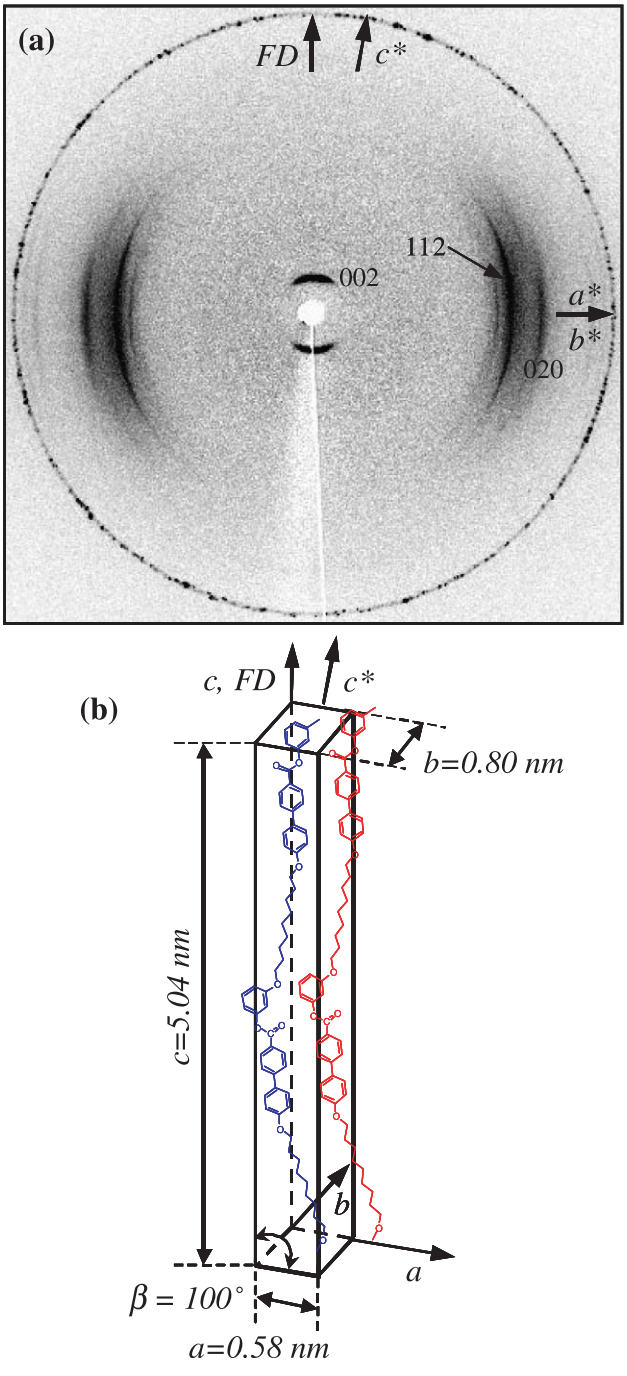

Fig. 4. 2D WAXD fiber pattern of the K_M crystalline phase of BPE-C9 after the sample was drawn in the LC phase at 177 °C and annealed at 158 °C for 1 day. The fiber draw direction and c-axis is along the meridian direction, but the c^*-axis is $\pm 10°$ away from meridian direction (a). The a^*- and b^*-axes are along the equatorial direction. A schematic unit cell model with two chains for the K_M crystalline phase of BPE-C9 (b).

Table 1
Experimental and calculated crystallographic parameters of the K_M crystalline phase of BPE-C9

hkl	2θ (°)		*d*-Spacing (nm)		Int[a]
	Expt[b]	Calc[c]	Expt[b]	Calc[c]	
020	22.1	22.2	0.40	0.40	vs
110	19.1	19.1	0.47	0.47	vs
$\bar{1}10$	19.1	19.1	0.47	0.47	vs
120	27.1	27.2	0.33	0.33	m
$\bar{1}20$	27.1	27.2	0.33	0.33	m
011	11.2	11.2	0.78	0.79	vw
002	3.56	3.56	2.47	2.48	vs
112	20.0	19.9	0.44	0.45	s
004	7.13	7.13	1.23	1.24	w

[a] The intensities are semiquantitatively estimated via a microdesitometer and classified as very strong (vs), strong (s), medium (m), weak (w), and very weak (vw).
[b] The accuracy of the experimental data is ± 0.005 nm.
[c] The calculated data listed are based on the K_M orthorhombic unit cell with $a = 0.58$ nm, $b = 0.80$ nm, $c = 5.04$ nm, $\alpha = \gamma = 90.0°$ and $\beta = 100.0°$.

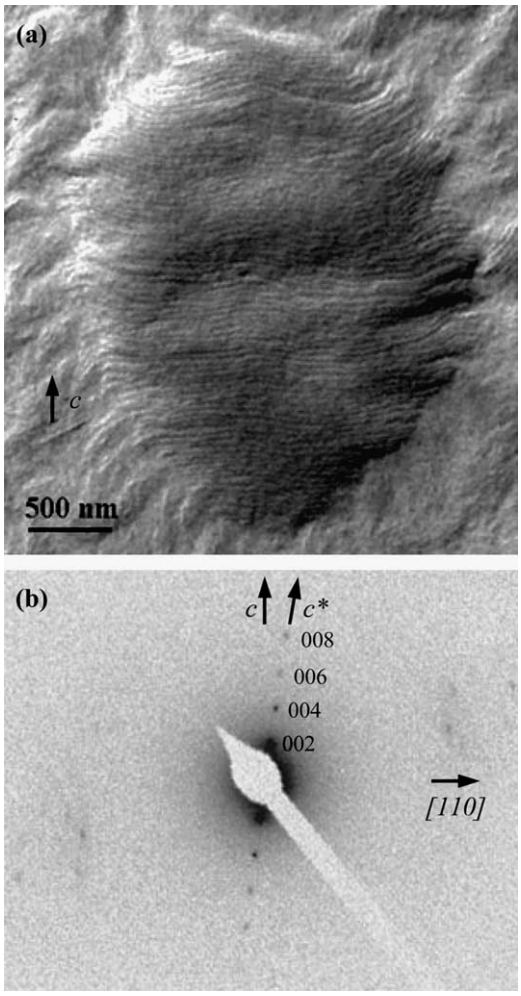

Fig. 5. TEM image of the edge-on lamellar crystal stack (a), SAED pattern of the [$\bar{1}$10] zone (b) without tilting obtained from the edge-on lamellar crystals of BPE-C9.

methylene units are all in the trans-conformation [12–18]. Odd-numbered BPE-C*n* polyesters have two possible bends: one is from the meta-linkage (configurational bend) at the end of the mesogenic groups, and the other is from the odd-number of methylene units in the spacers (conformational bend). Therefore, the opposite observation of the chain conformations in this series of BPE-C*n* should be attributed to the interplay between the mesogenic group ordering propensity and the chain constraints dictated by the methylene spacer and the meta-linkage at the end of mesogens.

This structural determination and schematic two-chain unit cell model for the K_M phase in BPE-C9 are supported by SAED experiments conducted on BPE-C9 single crystals in TEM. Fig. 5(a) shows a stack of edge-on lamellar crystals grown at a cooling rate of 0.1 °C/min from the I phase and annealed at 158 °C for 12 h under a dry nitrogen atmosphere. Without tilting this lamellar crystal stack, the SAED pattern is close to the [$\bar{1}$10] zone as shown in Fig. 5(b). Therefore, the strong X-ray (020) diffraction on the equator cannot be observed in this SAED. Since this [$\bar{1}$10] zone SAED pattern is from the well aligned stacked lamellae, a pair of (002) diffraction and its higher order diffractions at $+10°$ away from the *c*-axis (but not at $-10°$) appeared since the uniaxial orientation of the lamellar crystal stack. This agrees well with the results of the 2D WAXD (Fig. 4(a)). Inside of the K_M crystalline lattice of BPE-C9, detailed polymer chain packing information can be obtained from the [001] zone ED pattern, in which the electron beam enters along the chain direction. In order to obtain an ED pattern from the [001] zone, the BPE-C9 sample in the I phase was quenched to room temperature and annealed at 158 °C for 12 h. The resulting TEM morphology in Fig. 6(a) shows more or less flat-on lamellar crystals. The SAED from this lamellar crystal is from the [401] zone without sample tilting, as shown in Fig. 6(b). Only a pair of the (020) diffractions is observed. As shown in Fig. 6(c), the SAED pattern from the [00l] zone is obtained by tilting the sample 31° counter-clockwise around the *b**-axis from the [401] zone, which fully agrees with the polymer chain packing model presented in Fig. 4(b). The calculated γ angle (90°) from the triangulation method of building a 2D *a***b**-lattice of the unit cell in Fig. 4(a) is also confirmed by this [00l] zone SAED.

Fig. 7(a) shows a 2D WAXD fiber pattern for BPE-C7 from a fiber drawn in the LC phase at 190 °C and annealed at 185 °C for 1 day. The 2D WAXD fiber pattern of BPE-C7 is surprising since it is different from BPE-C9. In high 2θ-angle region, the *a**- and

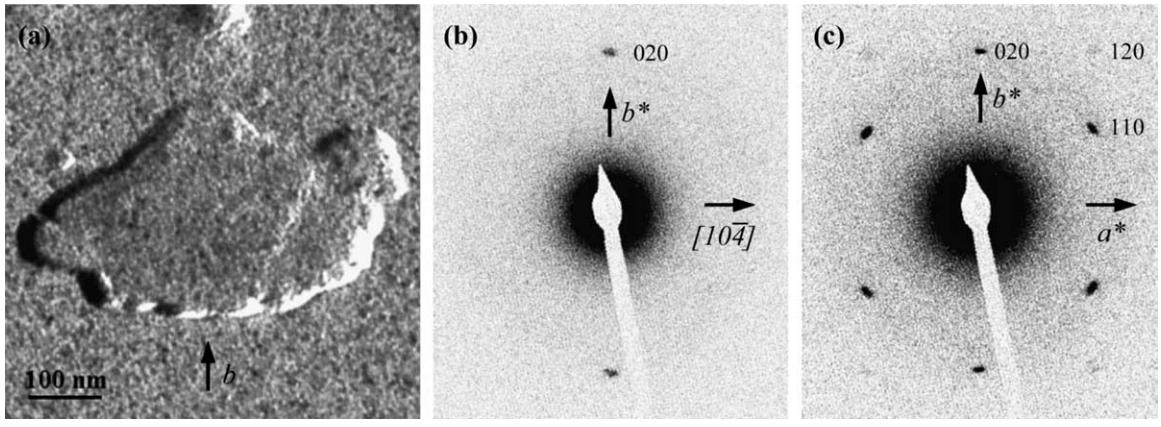

Fig. 6. TEM image of the flat-on single crystal (a), SAED patterns of the [401] zone (b), and the [001] zone (c) obtained from the more or less flat-on single lamellar crystal of BPE-C9. The [001] zone SAED pattern was obtained by 31°-counter-clockwise tilting of the [401] zone sample around *b**-axis.

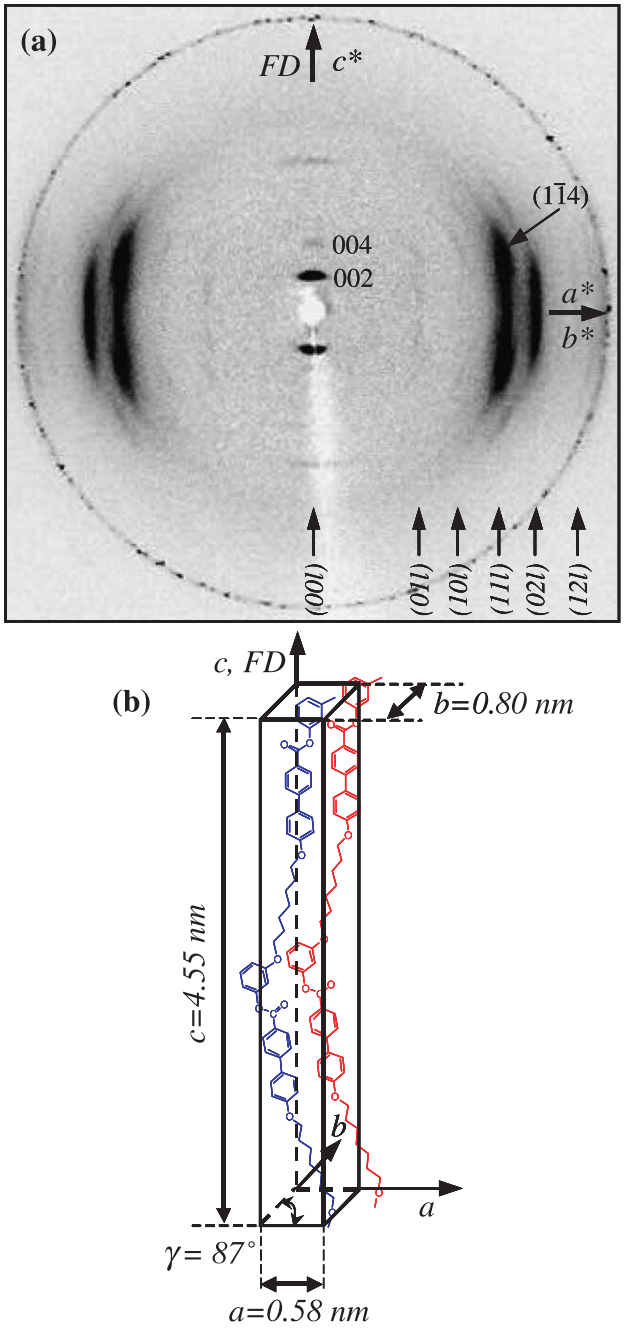

Fig. 7. 2D WAXD fiber pattern of the K_M crystalline phase of BPE-C7 after the sample was drawn in the LC phase at 190 °C and annealed at 185 °C for 1 day. The fiber drawn direction and c*-axis are along the meridian direction while the a*- and b*-axes are along the equatorial direction (a). A schematic unit cell model with two chains for the K_M crystalline phase of BPE-C7 (b).

b*-axes are assigned to the equator, while the c*-axis is along the fiber drawn direction (meridian). On the equator of this fiber pattern, two strong diffractions are located at $2\theta = 18.5°$ (d = 0.48 nm) and 22.4° (d = 0.40 nm) with two very weak diffractions at $2\theta = 15.2°$ (d = 0.58 nm) and 26.5° (d = 0.34 nm). They can be assigned as the (110), (020), (100) and (120) planes, respectively, based on the triangulation method of building a 2D a*b*-lattice of the unit cell [38]. Based on these diffraction spots on the equator, however, the γ* angle is

Table 2
Experimental and calculated crystallographic parameters of the K_M crystalline phase of BPE-C7

hkl	2θ (°)		*d*-Spacing (nm)		Int[a]
	Expt[b]	Calc[c]	Expt[b]	Calc[c]	
020	22.4	22.3	0.40	0.40	vs
110	18.5	18.4	0.48	0.48	w
011	11.3	11.3	0.78	0.78	w
111	18.6	18.5	0.48	0.48	vs
122	26.9	26.8	0.33	0.33	vw
013	12.5	12.6	0.71	0.70	w
113	19.3	19.3	0.46	0.46	vs
1$\bar{1}$4	20.9	20.9	0.43	0.43	m
104	17.1	17.1	0.52	0.52	w
106	19.2	19.2	0.45	0.46	w
002	3.88	3.88	2.27	2.28	vs
004	7.76	7.77	1.14	1.14	m

[a] The intensities are semiquantitatively estimated via a microdesitometer and classified as very strong (vs), strong (s), medium (m), weak (w), and very weak (vw).
[b] The accuracy of the experimental data is ±0.005 nm.
[c] The calculated data listed are based on the K_M orthorhombic unit cell with a = 0.58 nm, b = 0.80 nm, c = 4.55 nm, $\alpha = \beta = 90.0°$ and $\gamma = 87.0°$.

calculated to be 93°. In the low 2θ-angle region of this fiber pattern, a pair of strong diffraction spots on the meridian is at $2\theta = 3.88°$ (d = 2.27 nm) with higher order diffractions at 2θ = 7.76° (d = 1.14 nm) and 11.66° (d = 0.76 nm). They should be assigned as the (002), (004) and (006) planes for the same reasons as the series of BPE-Cn [30]. Careful structural analysis results in a monoclinic unit cell with dimensions of a = 0.58 nm, b = 0.80 nm, c = 4.55 nm, $\alpha = \beta = 90°$, and $\gamma = 87°$ via the refinement of the reciprocal lattice, and this phase is abbreviated as the K_M phase. Table 2 lists the experimentally observed and the calculated 2θ values and the d-spacings based on this unit cell lattice. With two chains (four chemical repeating units) in this monoclinic unit cell, its calculated crystallographic density is 1.27 g/cm^3. The experimentally observed density is 1.25 g/cm^3, which fits well with the calculated data. A schematic two-chain unit cell model for this K_M crystalline phase of BPE-C7 is shown in Fig. 7(b). The aromatic mesogenic groups in BPE-C7 are also more or less parallel to each other along the FD direction, but the γ angle is not 90° but 87°.

This structural determination and chain-packing model for the K_M phase in BPE-C7 are also supported by SAED experiments conducted on BPE-C7 single crystals in TEM. Fig. 8(a) shows a stack of edge-on lamellar crystals grown at a cooling rate of 0.1 °C/min from the I phase and annealed at 185 °C for 12 h under a dry nitrogen atmosphere. The [1$\bar{1}$0] zone SAED pattern is obtained without tilting the sample. The (002) and (004) diffractions are along the lamellar normal direction, that is, the polymer chain long axis is parallel to the thickness direction of the lamellar single crystals. The BPE-C7 sample in the I phase was quenched to room temperature and annealed at 185 °C for 12 h. Fig. 9(a) shows flat-on lamellar crystal morphology in TEM. As shown in Fig. 9(b), the [001] zone SAED is obtained without tilting the flat-on lamellar crystal, which fully agrees with the polymer chain-packing model presented in Fig. 7(b). The calculated γ* angle (93°)

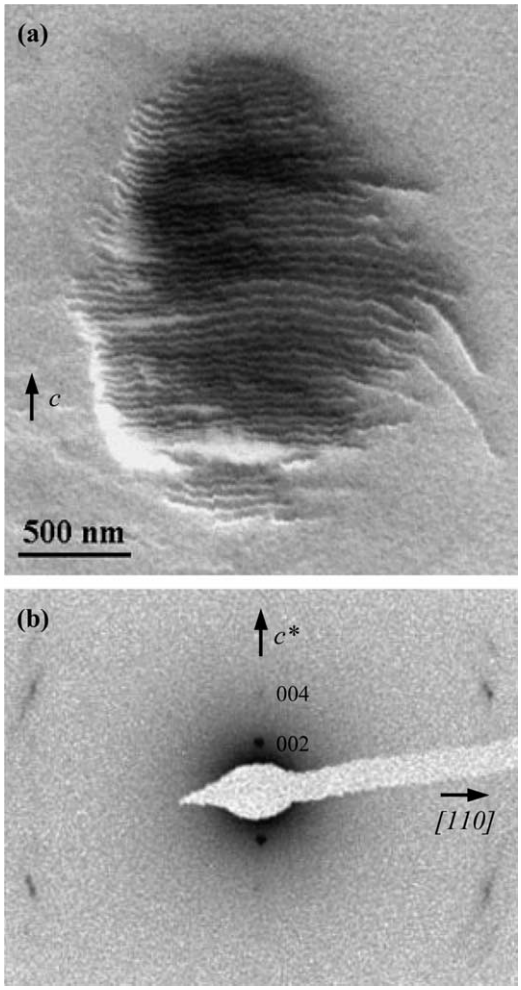

Fig. 8. TEM image of the edge-on lamellar crystal stack (a) and SAED pattern of the [$\bar{1}$10] zone (b) without tilting obtained from the edge-on lamellar crystals of BPE-C7.

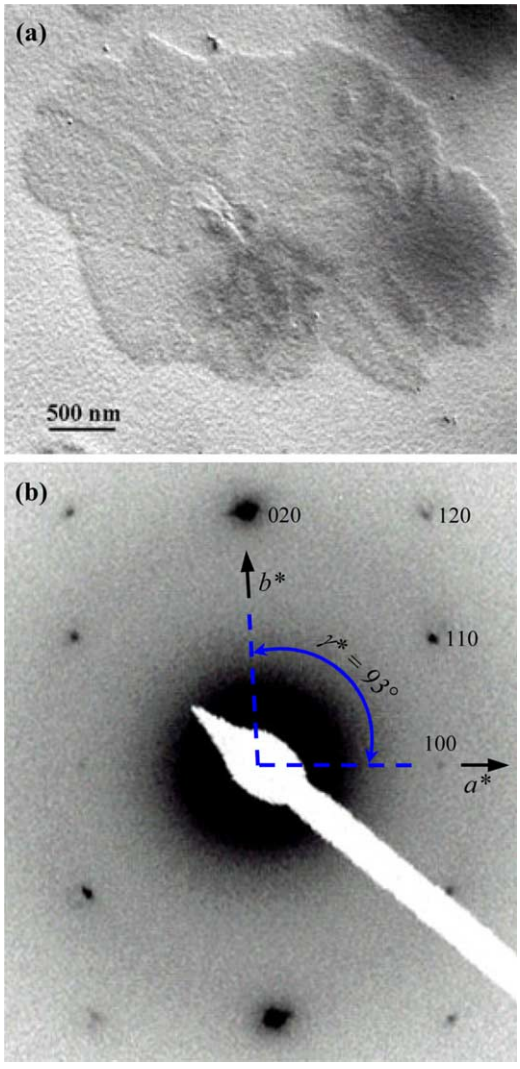

Fig. 9. TEM image of the flat-on single crystal (a), and SAED pattern of the [001] zone (b) for the flat-on single lamellar crystal of BPE-C7. The [001] zone SAED pattern was obtained without sample tilting.

from the triangulation method of building a 2D a^*b^*-lattice of the unit cell in Fig. 7(a) is also confirmed from this [00l] zone SAED.

Molecular packing features of the main-chain LC polymers arise from the interplay between the ordering propensity driven by the interactions among the mesogenic groups and the intra/inter chain constraints dictated by the spacers connecting the mesogenic groups [1,2]. The different crystalline structures of BPE-C*n* between $n=7$ and 9 could be attributed to the spatial chain conformations with different lengths of the methylene spacers and the effect of the meta-linkage at the end of mesogens, which compete with the effective close packing. In order to study the interplay and to confirm the structures of the K_M crystalline phases in these two odd-numbered BPE-C*n*, computer calculations were carried out using Cerius^2 (Version 4.6) software, and which can generate a detailed chain-packing scheme. In order to examine whether the proposed packing scheme fits to the real structure, the calculated diffraction patterns are generated and compared with the experimentally obtained diffraction patterns. First, the global equilibrium conformations of the monomers (BPCA-C*n*-P*m*OH, $n=7$ and 9) were constructed at 0 K using the COMPASS force-field. The energy-minimized monomers were used to construct the BPE-C*n* polyesters. The lowest energy conformation of each single polymer chain was chosen as the starting conformation. Basic unit cell parameters determined by experimental data from 2D WAXD and SAED experiments were used to build the K_M structures. Figs. 10(a) and 11(a) show the two-chain packing schemes for BPE-C9 and BPE-C7, respectively, suggested by the computer calculations with side (the [010] zone, Figs. 10(b) and 11(b)) and top (the [001] zone, Figs. 10(c) and 11(c)) views. The calculated 2D WAXD fiber patterns (Figs. 10(d) and 11(d)) and SAED pattern with the [001] zone (Figs. 10(e) and 11(e)) based on these schemes, respectively, which are qualitatively matched with the experimental observations (Figs. 4(a) and 6(c) for BPE-C9, and Figs. 7(a) and 9(b) for BPE-C7). For the close packing of two odd-numbered BPE-C*n* during crystallization, the chain conformations are not in the (0*k*0) planes unlike the zigzag conformation in the even-numbered BPE-C*n* [30]. Therefore,

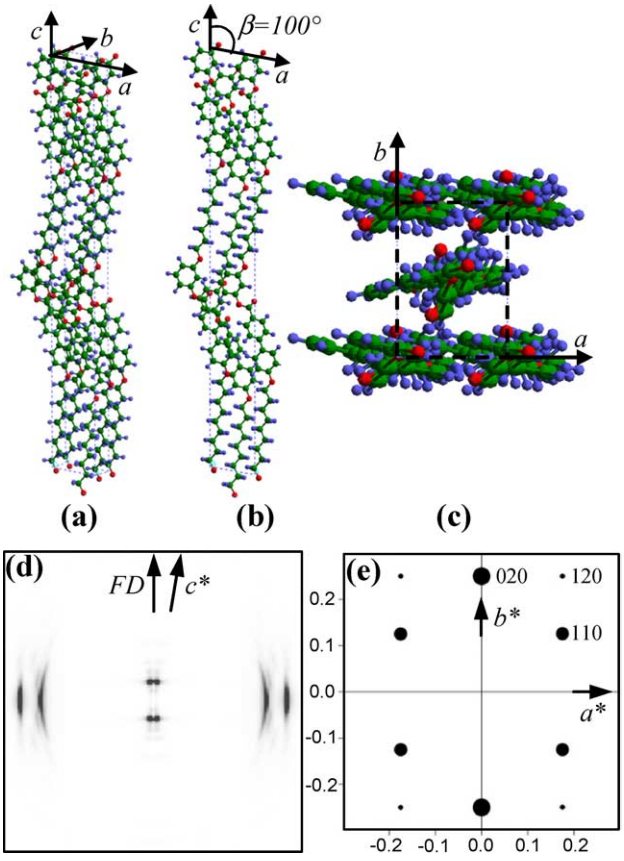

Fig. 10. Computer simulated BPE-C9 chain packing scheme in the unit cell with the best match to the experimental 2D WAXD and SAED patterns (a) with views from the side (the [010] zone) (b) and the top (the [001] zone) (c). Computer calculated 2D WAXD pattern (d) and SAED pattern of the [001] zone (e), which agree well with those of the experimental 2D WAXD (Fig. 4(a)) and SAED (Fig. 6(c)) diffraction patterns.

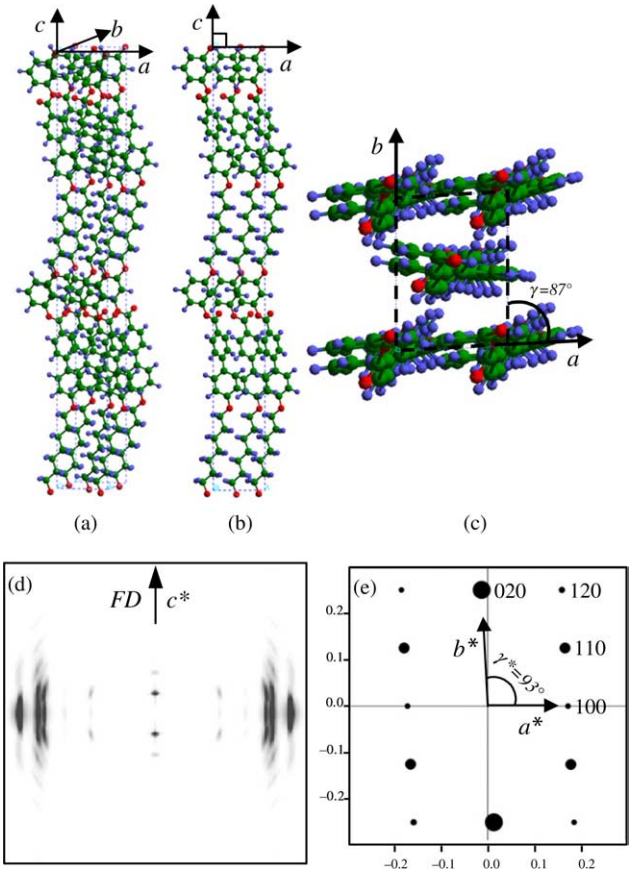

Fig. 11. Computer simulated BPE-C7 chain packing scheme in unit cell with the best match to the experimental 2D WAXD and SAED patterns (a) with views from the side (the [010] zone) (b) and the top (the [001] zone) (c). Computer calculated 2D WAXD pattern (d) and SAED pattern of the [001] zone (e), which agree well with those of the experimental 2D WAXD (Fig. 7(a)) and SAED (Fig. 9(b)) diffraction patterns.

the resulting herringbone-like packing of the chains distorts the lattice to become a monoclinic unit cell (K_M). BPE-C9 possessed a $\beta = 100°$ by translating the chains along the *c*-axis (~0.5 nm, Fig. 10(b)), while BPE-C7 possessed a $\gamma = 87°$ by distorting the *ab*-lattice (Fig. 11(c)).

3.3. Identification of liquid crystal structures

The structure of the low-ordered LC phase observed between 181 and 160 °C can also be identified using the 2D WAXD fiber pattern of BPE-C9 as shown in Fig. 12(a). The oriented BPE-C9 fiber sample was prepared by drawing in the LC phase and annealing at 177 °C for 2 h under a dry nitrogen atmosphere. This figure shows a pair of scattering halos at $2\theta = 19.4°$ ($d = 0.46$ nm), where its maximum intensity is on the equator with a correlation length of ~2.2 nm as estimated by the Scherrer equation. A pair of low 2θ-angle diffraction spots appears on the meridian at $2\theta = 3.70°$ ($d = 2.39$ nm) with a high order diffraction at $2\theta = 7.40°$ ($d = 1.20$ nm), indicating that the layer normal is along the FD direction. Therefore, this low-ordered LC phase can be identified as a SmA phase [36,37], as illustrated in Fig. 12(b). It is predicted that the overall chain long axis in the drawn polymer fiber sample in this low-ordered LC phase change is parallel to the layer normal during the transition from the K_M crystalline phase. The measured layer thickness (2.39 nm) is shorter than the calculated length of the chain (2.61 nm). This difference may be due to the fact that the alkoxyl chains of BPE-C9 in this SmA phase contain local gauche and trans conformations instead of the assumed all-trans conformation in the calculation [39–43].

The 2D WAXD fiber pattern of the BPE-C7 sample is similar to that of BPE-C9 (Fig. 12(a)), and it is also identified as a SmA phase. The layer diffraction of this SmA phase for BPE-C7 is at $2\theta = 4.02°$ ($d = 2.20$ nm). When the layer thicknesses were considered in the series of BPE-C*n* from $n = 6$ to 10, the structural odd–even effect can be identified: 2.01 nm ($n = 6$), 2.20 nm ($n = 7$), 2.18 nm ($n = 8$), 2.39 nm ($n = 9$), and 2.38 ($n = 10$). This structural odd–even effect is due to the fact that odd-numbered BPE-C*n* exhibit a SmA phase while even-numbered BPE-C*n* exhibit an anticlinically tilted SmC (SmC_A) phase [30]. In addition, odd-numbered BPE-C*n* do not show the highly ordered LC phase (SmH) observed in the even-numbered BPE-C*n* [30].

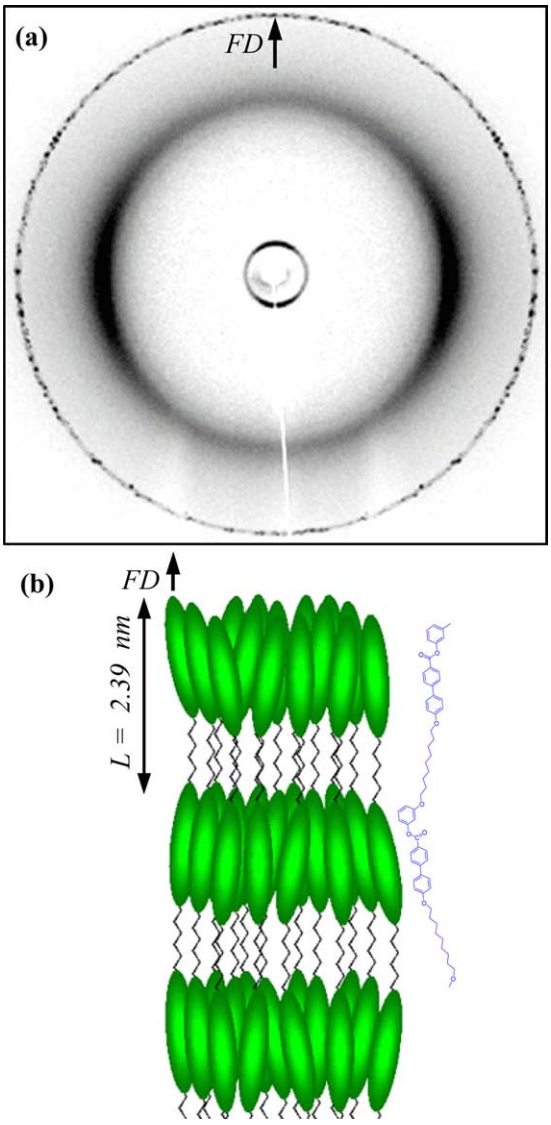

Fig. 12. 2D WAXD fiber pattern of the low-ordered SmA LC phase of BPE-C9 after the sample was annealed at 177 °C for 2 h. The fiber draw direction is along the meridian (a). A schematic chain-packing model for the SmA LC phase of BPE-C9 (b).

3.4. Liquid crystalline textures

The phase identifications of odd-numbered BPE-C*n* polyesters based on diffraction methods combined with DSC results can also be supported by the observation of texture changes in PLM at the transitions. Fig. 13(a) and (b) show changes in the BPE-C9 morphological textures upon cooling. At a cooling rate of 0.1 °C/min, the transition from the I phase to the SmA phase occurs at 181 °C. At this point a bâtonnet texture against the I phase can be observed, which is often observed in the smectic LC phases (Fig. 13(a)) [44,45]. When the temperature reaches 160 °C, this sample is crystallized, as shown in Fig. 13(b). Odd-numbered BPE-C*n* do not show any ring striation, an indication of no chain tilting in BPE-C7 as well as BPE-C9, and thus no SmC

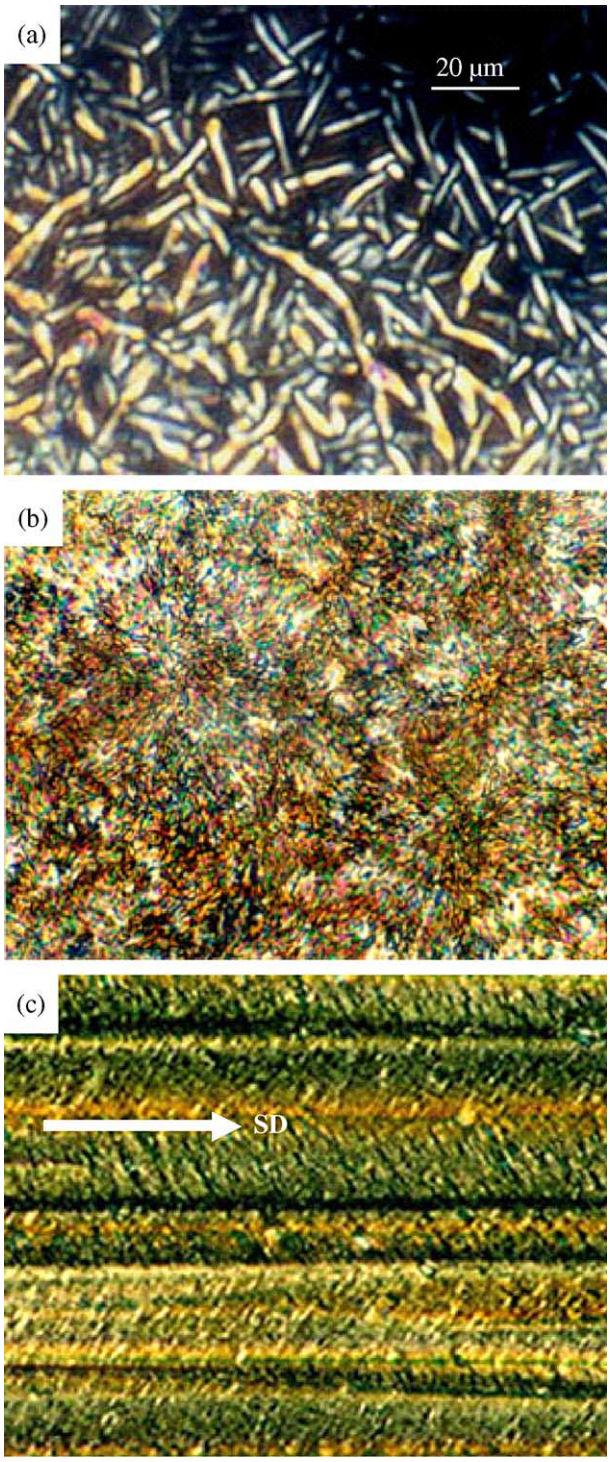

Fig. 13. Morphological observations of BPE-C9 in PLM at two temperatures at a cooling rate of 0.1 °C/min: the SmA phase at 177 °C (a), and the K_M phase at 30 °C (b). PLM morphological observations of the BPE-C9 sample after mechanical shearing in the SmA phase (c). The arrow represents the shear direction.

phase formation. In the even-numbered BPE-C*n*, on the other hand, ring striations do form [30]. Fig. 13(c) shows a cluster of oriented bâtonnet-like textures induced by mechanical shearing of the sample in the SmA phase, similar to the

observations previously reported [30,45]. The chain orientation is parallel to the shear direction. When this sample is annealed more than 10 h in the SmA phase under a dry nitrogen atmosphere, bigger elongated bâtonnet texture domains appear, similar to the PLM image as shown in Fig. 13(a).

In the odd-numbered BPE-C*n*, there is neither the helical supra-molecular texture (which exists in BPCA-C*n*-P*m*OH, its monomer) [28,29], nor the ring striation with three different colors (which are observed in the corresponding even-numbered BPE-C*n*) [30]. This is because that the odd-numbered BPE-C*n* have neither a large zigzag conformation in their polymer chains nor a continuous twisting of the chemical repeat unit from one to another along the same twisting direction. Furthermore, the SmC phase does not exist in these two odd-numbered BPE-C*n* polyesters. Therefore, no SmA to SmC phase transition takes place.

4. Conclusion

Two new asymmetric odd-numbered main-chain LC polyesters (BPE-C*n*) synthesized through the condensation polymerization of the A–B type asymmetric BPCA-C*n*-P*m*OH monomers containing different numbers of methylene spacers ($n=7$ and 9) exhibit two different phases as observed via DSC and 1D WAXD measurements. Based on 2D WAXD and SAED results, these two phases are identified to be the low-ordered SmA phase and the monoclinic crystalline (K_M) phases. Chain-packing schemes for the crystalline phases (K_M) have been proposed based on the experimental diffraction patterns and qualitatively supported using simulated structural diffractions. These K_M crystal unit cells consist of four chemical repeating units. The K_M of BPE-C9 possessed a $\beta=100°$, while BPE-C7 had a $\gamma=87°$. In the ordered phases of these two odd-numbered BPE-C*n*, the aromatic mesogenic groups are more or less parallel to each other along the chains, different from those large zigzag conformation structures in even-numbered BPE-C*n* crystals. These forms accommodate the bend from the odd-numbered methylene spacers and the bend caused by the configurational meta-linkage at the end of the mesogenic groups. The LC morphological transformations were also identified via PLM. Since, the odd-numbered BPE-C*n* samples have neither a large zigzag conformation in their polymer chains unlike the even-numbered BPE-C*n*, nor a continuous twisting of the chemical repeat unit from one to another along the same twisting direction as in the case of their corresponding monomers, there is no helical supra-molecular structures nor ring striation.

Acknowledgements

This work was supported by the National Science Foundation (DMR-0516602). We also acknowledge Perkin–Elmer Co. for their support in providing a Diamond DSC instrument for our laboratory.

References

[1] Greiner A, Schmidt H-W. In: Demus D, Goodby J, Gray GW, Spiess H-W, Vill V, editors. Handbook of liquid crystals, vol. 3. Weinheim: Wiley–VCH; 1998. p. 3–25.
[2] Chiellini E, Laus M. In: Demus D, Goodby J, Gray GW, Spiess H-W, Vill V, editors. Handbook of liquid crystals, vol. 3. Weinheim: Wiley–VCH; 1998. p. 26–51.
[3] Bello A, Riande E, Pérez E, Marugán MM, Pereña JM. Macromolecules 1993;26:1072.
[4] Orifici AF, Vallés EM, Garay RO, Lenz RW. Polymer 1996;37:4357.
[5] Jehnichen D, Friedel P, Bergmann J, Taut T, Tobisch J, Pospiech D. Polymer 1998;39:1095.
[6] Ge JJ, Zhang A, McCreight KW, Ho R-M, Wang S-Y, Jin X, et al. Macromolecules 1997;30:6498.
[7] Ge JJ, Zhang A, McCreight KW, Wang S-Y, Harris FW, Cheng SZD. Macromolecules 1998;31:4093.
[8] Ge JJ, Honigfort PS, Ho R-M, Wang S-Y, Harris FW, Cheng SZD. Macromol Chem Phys 1999;200:31.
[9] Ge JJ, Guo M, Zhang Z, Honigfort PS, Wang S-Y, Harris FW, et al. Macromolecules 2000;33:3983.
[10] Ruan J, Ge JJ, Zhang A, Jin S, Wang S-Y, Harris FW, et al. Macromolecules 2002;35:736.
[11] Hu YS, Liu RYF, Schiraldi DA, Hiltner A, Baer E. Macromolecules 2004;37:2128.
[12] Watanabe J, Hayashi M. Macromolecules 1988;21:278.
[13] Watanabe J, Hayashi M. Macromolecules 1989;22:4083.
[14] Watanabe J, Nakata Y, Simizu K. J Phys II 1994;4:581.
[15] Watanabe J, Hayashi M, Morita A, Tokita M. Macromolecules 1995;28:8073.
[16] Tokita M, Takahashi T, Hayashi M, Inomata K, Watanabe J. Macromolecules 1996;29:1345.
[17] Osada K, Niwano H, Tokita M, Kawauchi S, Watanabe J. Macromolecules 2000;33:7420.
[18] Tokita M, Tokunaga K, Funaoka S, Osada K, Watanabe J. Macromolecules 2004;37:2527.
[19] Li CY, Yan D, Cheng SZD, Bai F, He T, Chien LC, et al. Macromolecules 1999;32:524.
[20] Li CY, Yan D, Cheng SZD, Bai F, Ge JJ, Calhoun BH, et al. Phys Rev B 1999;60:12675.
[21] Li CY, Cheng SZD, Ge JJ, Bai F, Zhang JZ, Mann IK, et al. Phys Rev Lett 1999;83:4558.
[22] Li CY, Ge JJ, Bai F, Zhang JZ, Calhoun BH, Chien LC, et al. Polymer 2000;41:8953.
[23] Li CY, Cheng SZD, Ge JJ, Bai F, Zhang JZ, Mann IK, et al. J Am Chem Soc 2000;122:72.
[24] Li CY, Cheng SZD, Weng X, Ge JJ, Bai F, Zhang JZ, et al. J Am Chem Soc 2001;123:2462.
[25] Li CY, Ge JJ, Bai F, Calhoun BH, Harris FW, Cheng SZD, et al. Macromolecules 2001;34:3634.
[26] Li CY, Jin S, Weng X, Ge JJ, Zhang D, Bai F, et al. Macromolecules 2002;35:5475.
[27] Weng X, Li CY, Jin S, Zhang JJ, Zhang D, Harris FW, et al. Macromolecules 2002;35:9678.
[28] Jeong KU, Jin S, Ge JJ, Knapp BS, Graham MJ, Ruan J, et al. Chem Mater 2005;17:2852.
[29] Jeong KU, Knapp BS, Ge JJ, Jin S, Graham MJ, Harris FW, et al. Chem Mater 2006;18:680.
[30] Jeong KU, Knapp BS, Ge JJ, Jin S, Graham MJ, Xiong H, et al. Macromolecules 2005;38:8333.
[31] Knapp BS. PhD Dissertation. University of Akron; 2003.
[32] Pardey R, Shen D, Gabori PA, Harris FW, Cheng SZD, Adduci J, et al. Macromolecules 1993;26:3687.
[33] Yoon Y, Zhang A, Ho R-M, Cheng SZD, Percec V, Chu P. Macromolecules 1996;29:294.
[34] Yoon Y, Ho R-M, Moon B, Kim D, McCreight KW, Li F, et al. Macromolecules 1996;29:3421.

[35] Zheng R-Q, Chen E-Q, Cheng SZD, Xie F, Yan D, He T, et al. Macromolecules 1999;32:6981.
[36] Demus D. In: Demus D, Goodby J, Gray GW, Spiess H-W, Vill V, editors. Handbook of liquid crystals, vol. 1. Weinheim: Wiley–VCH; 1998. p. 133–87.
[37] Seddon JM. In: Demus D, Goodby J, Gray GW, Spiess H-W, Vill V, editors. Handbook of liquid crystals, vol. 1. Weinheim: Wiley–VCH; 1998. p. 635–79.
[38] Eashoo M, Wu Z, Zhang A, Shen D, Tse C, Harris FW, et al. Macromol Chem Phys 1994;195:2207.
[39] Bovey FA, Mirau PA. NMR of polymers. San Diego: Academic Press; 1996.
[40] Cheng J, Jin Y, Wunderlich B, Cheng SZD, Yandrasits MA, Zhang A, et al. Macromolecules 1992;25:5991.
[41] Cheng J, Yoon Y, Ho R-M, Leland M, Guo M, Cheng SZD, et al. Macromolecules 1997;30:4688.
[42] McElheny D, Grinshtein J, Frydman V, Frydman L. Macromolecules 2002;35:3544.
[43] Ishida H, Horii F. Macromolecules 2002;35:5550.
[44] Dierking I. Textures of liquid crystals. Weinheim: Wiley–VCH; 2003.
[45] Krigbaum WR, Watanabe J. Polymer 1983;24:1299.